

Simulation of humpback whale bubble-net feeding models

Spencer H. Bryngelson^{a)} and Tim Colonius

Division of Engineering and Applied Science, California Institute of Technology,

1200 E California Blvd, Pasadena, CA 91125, USA

1 Humpback whales can generate intricate bubbly regions, called bubble nets, via their
2 blowholes. They appear to exploit these bubble nets for feeding via loud vocalizations.
3 A fully-coupled phase-averaging approach is used to model the flow, bubble dynamics,
4 and corresponding acoustics. A previously hypothesized waveguiding mechanism is
5 assessed for varying acoustic frequencies and net void fractions. Reflections within
6 the bubbly region result in observable waveguiding for only a small range of flow
7 parameters. A configuration of multiple whales surrounding and vocalizing towards
8 an annular bubble net is also analyzed. For a range of flow parameters the bubble net
9 keeps its core region substantially quieter than the exterior. This approach appears
10 more viable, though it relies upon the cooperation of multiple whales. A spiral bubble
11 net configuration that circumvents this requirement is also investigated. The acoustic
12 wave behaviors in the spiral interior vary qualitatively with the vocalization frequency
13 and net void fraction. The competing effects of vocalization guiding and acoustic
14 attenuation are quantified. Low void fraction cases allow low-frequency waves to
15 partially escape the spiral region, with the remaining vocalizations still exciting the
16 net interior. Higher void fraction nets appear preferable, guiding even low-frequency
17 vocalizations while still maintaining a quiet net interior.

a)spencer@caltech.edu

¹⁸ I. INTRODUCTION

¹⁹ Humpback whales (*Megaptera novaeangliae*) utilize sophisticated underwater feeding
²⁰ strategies¹⁴. They can generate bubbles with their dorsal surface (blowholes) and form
²¹ bubble columns¹³, clouds¹³, and nets¹⁵ with complex swimming maneuvers¹¹. The whales
²² appear to leverage these bubbly regions via acoustic excitation for trapping and corralling
²³ small fish (mostly herring and krill¹³). Indeed, the whale vocalization frequencies often even
²⁴ overlap with the resonant frequencies of the fish swim bladders^{17,21}. However, the mecha-
²⁵ nisms by which the whales exploit (or suffer from²³) these nets are generally unknown. The
²⁶ bubble-net feeding strategy is focused on here, for which the whales swim downwards in a
²⁷ circular motion, starting from a few meters below the ocean surface. They then rotate their
²⁸ blowholes towards the will-be bubble-net center and release several “bursts” of bubbles¹³,
²⁹ creating an annular or spiral cylinder of bubbles²⁹ as shown in figure 1 (a) and (b). From the
³⁰ net exterior, from one to about 15³² whales ~~generate-vocalize, generating~~ a loud trumpeting
³¹ sound. A model of four whales vocalizing towards such a net is shown in figure 1 (b). The
³² whales then rise within the net center and consume their prey in a process called vertical
³³ lunge feeding⁸ (see figure 1 (c)).

³⁴ Observations of bubble nets are scarce, as they usually occur in isolated ocean areas. As a
³⁵ result, hypotheses of how whale generated acoustic waves and their interactions with bubble
³⁶ nets result in advantageous feeding strategies are broad. For example, it is possible that
³⁷ whales utilize their nets to echolocate prey²⁶, though this could require higher frequencies
³⁸ than those usually observed during the bubble-net feeding process. ~~Here, the possibility~~ It

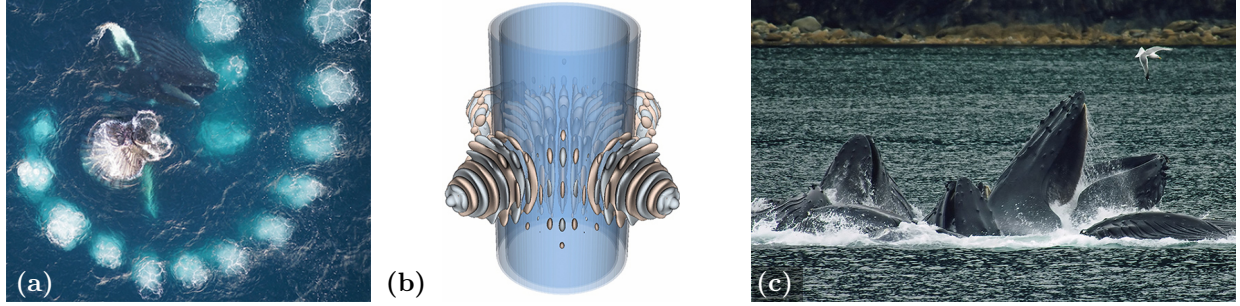


FIG. 1. (a) Aerial view of a humpback whale bubble net⁷, (b) visualization of four whales vocalizing towards a bubble net using the present simulation method (see section II), and (c) several humpback whales lunge feeding⁹.

39 is also possible that the whales attempt to surround ~~and trap~~ their prey with loud vocaliza-
 40 tions~~is considered for~~. If the vocalizations are loud enough, which is thought to be the case
 41 for humpback whale trumpeting calls³⁰, then the prey will be preferentially corralled into
 42 the net center or prohibited from leaving this region. We consider this possibility herein for
 43 different acoustic mechanisms. The viability of each mechanism has consequences beyond
 44 just the motives and behaviors of humpback whales. For example, similar phenomena can
 45 occur within the bubble curtains used to attenuate the underwater sound generated by
 46 pile-driving³⁴ and explosives⁶.

47 The first mechanism considered follows from Leighton¹⁸, who showed that the bubbly
 48 region could behave as a waveguide for the whale vocalizations if certain criteria are met.
 49 For this, the acoustic waves would enter (via refraction) and reflect within an annular bubbly
 50 region, eventually occupying the entire bubble net and ~~trapping the prey within a wall of~~
 51 surrounding the prey with loud sound. However, for this to be possible, the vocalizations
 52 must be focused in a sufficiently narrow angular range, the bubble natural frequency must be

53 higher than the vocalization frequency, and the sound must remain sufficiently directional
54 within the net²². While these criteria are plausible, it is unknown if geometric effects or
55 nonlinear and collective bubble interactions or oscillations will preclude a useful degree of
56 waveguiding. Indeed, Leighton *et al.*²¹ later hypothesized that it is improbable these criteria
57 could be reliably and simultaneously met, though it remains unclear if this mechanism is
58 physically viable for reasonable model parameterizations.

59 If the net geometry is annular, then it is possible that the bubble net simply shields
60 the interior from the vocalizations, which then surround the net region¹⁷. Bubble curtains
61 have been used to shield krill from damage in captivity¹⁰ and herring are reluctant to cross
62 high void fraction bubble curtains even in the absence of acoustic excitation²⁹. Thus, if the
63 effective impedance of the bubble net is large and acoustic refraction is insignificant, then
64 this conjecture is plausible. However, a ready assessment of this appears to be precluded by
65 the non-uniform void fraction within the net, acoustic interactions between multiple whales,
66 and geometric effects of the circular bubbly region.

67 More recently, it was noticed that the nets might instead have spiral shapes¹⁹. Other
68 acoustic mechanisms are possible if this is the case. For example, Leighton *et al.*²⁰ described
69 that the whales could reflect their vocalizations within the bubble-free region of the net,
70 which might allow a single whale to surround the entire net region with sound. Further,
71 this would utilize a larger fraction of the energy they generate, instead of squandering the
72 portion that is reflected away from the net in the waveguide scenario²¹. However, like above,
73 it is challenging to anticipate and confirm a full operating mechanism via only theoretical

⁷⁴ and ray-tracing analysis due to the non-uniform bubbly regions, collective bubbly effects,
⁷⁵ low-frequency behaviors, and the sum-and-difference frequencies that could arise.

⁷⁶ As a step towards understanding this feeding strategy, the present goals are to determine if
⁷⁷ a waveguiding behavior can be observed, to what degree the interior of the bubble net is kept
⁷⁸ quiet when directly excited by loud vocalizations, and the acoustic behavior and attenuation
⁷⁹ for spiral net configurations. It is possible to perform *in situ* or laboratory experiments to
⁸⁰ analyze such configurations. For example, Leighton *et al.*¹⁹ used expanded polystyrene to
⁸¹ model the acoustic impedance. However, it remains challenging to reliably control the bubble
⁸² population distribution or accurately observe the reflection and refractions that occurs near
⁸³ the bubble wall. This motivates the use numerical simulations to consider a range of possible
⁸⁴ flow parameters (net void fraction, vocalization frequency and orientation, etc.) and net
⁸⁵ geometries. Here, the simulation model used includes bubble–bubble interactions, nonlinear
⁸⁶ bubble dynamics including surface tension, viscosity, and mass transfer, geometric effects
⁸⁷ due to the bubble-net wall thickness, and the finite breadth of the driving acoustics. This
⁸⁸ model and the numerical methods used for its solution are described in greater detail in
⁸⁹ section II. Results are presented in section III for acoustically excited circular and spiral
⁹⁰ bubble nets for a range of model and flow parameters. The implications of these results are
⁹¹ discussed in section IV.

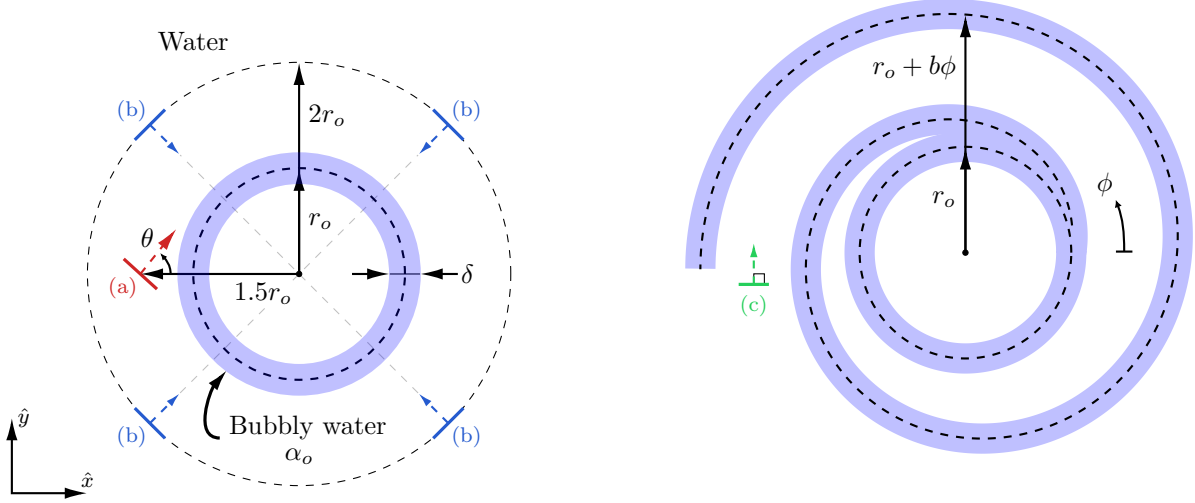


FIG. 2. Problem setups: Annular (left) and spiral bubble-nets (right). The lines (a–c) indicate different acoustic source locations and directions (see text).

⁹² II. MODEL SYSTEM AND NUMERICAL METHODS

⁹³ A. Problem setup

Schematics of the problems considered are shown in figure 2. The nominal height of the bubble net is at least as large as its nominal radius³³, so the bubble net flow system is modeled as two dimensional on average, though the individual bubbles are spherical. This model does not account for some of the more intricate upward spiral or double-loop three-dimensional bubble net geometries that have been reported³³, nor buoyant effects due to rising bubbles. Instead, it is utilized to test the hypotheses discussed in section I. These simplifications are further justified by the long buoyant advection times experienced by the small bubbles when compared to the short times (< 1 s) required for the whale vocalizations to propagate through the bubble net. The net region is either an annulus of radius r_o and

nominal thickness δ (figure 2, left) or the same annulus with the addition of an Archimedean spiral of radius $r = r_o + b\phi$, turning parameter $b = r_o/\pi$, and the same thickness (figure 2, right). Net parameters $r_o = 10$ m and $\delta = 4$ m are used, ~~both of which are reasonable estimates for~~. These choices follow from D'Vincent *et al.*⁸, though variations in net size have been observed and appear to be associated with the size of the whale that generates it. This idealized model does not attempt to represent the individual bubble columns of actual bubble nets ⁸ (visible in figure 1 (a)). Actual nets can also change shape as the whales interact with them, but the time scales of these interactions are much longer (longer than a few minutes^{8,13} than the acoustical phenomena we analyze here). The net is ~~located~~ fixed at the center of a side-length $L = 6r_o$ square domain. It is filled with spherical gas bubbles of density $\rho_g = 1$ kg/m³ and radius $R_o = 1$ mm, which follows from the ~~approxmimation~~ approximation of Wiley *et al.*³³, though variations of these parameters will be discussed. The bubbly water has void fraction α that varies with radial coordinate r up to its initial maximum value α_o at $r = r_o$ via a Gaussian bump as

$$\alpha(r) = \alpha_o \exp\left(-\frac{1}{2} \frac{(r - r_o)^2}{\sigma_\delta^2}\right), \quad (1)$$

where $\sigma_\delta = \delta/3$. ~~It is unclear what bubble void fractions humpback whales can create with their blowholes, particularly for bubble-net feeding purposes. For this reason, we consider a wide range of void fractions $\alpha_o \in (10^{-5}, 10^{-2})$ herein.~~ The domain is otherwise occupied with ~~pure~~ water of density $\rho_l = 998$ kg/m³. Note that we do not attempt to approximate the density of surface seawater (or spatial density variations due to salinity concentrations). However, our conclusions are insensitive to the small density variations (less than 2%) that such salinity entails.

101 Whale vocalizations are represented as one-way waves emitted from a line-source ~~of length~~
102 $L_a = 0.2r_o$ at a specified angle θ , frequency f , and ~~amplitude~~ peak sound pressure level (SPL)
103 at the source location A . The source has length $L_a = 0.2r_o$, which could be considered a
104 proxy for the lateral size of a humpback whale, though our conclusions are insensitive to
105 both doubling and halving this length. Humpback whales can produce complex sounds
106 ranging from 10 Hz to 30 kHz^{25,26}, though the trumpeting calls associated with bubble net
107 feeding are usually centered around a few kilohertz³⁰. Constructive sum-and-difference
108 frequencies could also extend the effective frequency observed at the bubble-net wall¹⁸.
109 Thus, a frequency range of Instead of considering actual whale vocalization recordings, a
110 monochromatic sine wave of frequencies $f = 0.1 \text{ kHz}$ to 5 kHz will be discussed herein are
111 used to assess the possibility of various acoustical phenomena. For the bubble sizes consid-
112 ered, this corresponds to both attenuated and enhanced effective mixture sound speeds in
113 the bubbly region⁴. The sound pressure peak SPL of the vocalizations is about at the source
114 location is $A = 180 \text{ dB re } 1 \mu\text{Pa}$ ³⁰, which is used here. These sounds usually last for as
115 an approximation of the $160 - 190 \text{ dB re } 1 \mu\text{Pa}$ at 1 m vocalizations that actual humpback
116 whales make during feeding³⁰. However, our conclusions were unchanged when considering
117 peak source pressures of $170 \text{ dB re } 1 \mu\text{Pa}$ and $190 \text{ dB re } 1 \mu\text{Pa}$. These sounds can last for
118 up to minutes⁸, which is much longer than the single-bubble-oscillation time scales. Thus,
119 the acoustics-generating sources are active for the duration of the simulations.

120 The locations of the acoustic line sources are shown in figure 2. The first configuration,
121 shown in figure 2 (a), is a single line source with angle $\theta = 50^\circ$ from the \hat{x} -direction, which
122 is used to determine if a waveguiding behavior can be observed in the bubbly region. The

123 second configuration (figure 2 (b)) is N_w line sources ($N_w = 4$ shown), each $2r_o$ from and di-
 124 rected towards the bubble net center, which is used to assess the effective acoustic impedance
 125 of the bubble net. These locations are based off of observations of whales vocalizing within
 126 a few net radii³³; though our conclusions are insensitive to their precise position. Actual
 127 whales are also unlikely to be azimuthally-equidistant, though this idealized configuration
 128 provides a means of assessing the possibility of various acoustical behaviors. The last con-
 129 figuration, shown in figure 2 (c), is a single line source of angle $\theta = 90^\circ$, directed into the
 130 bubble-free arm of a spiral bubble net. Note that these sources are fixed in space, and thus
 131 Doppler effects are not considered. However, the broad frequency range considered, along
 132 with the relative insensitivity of the results near the ends of this range, confirms that such
 133 effects are insignificant for current purposes.

134 B. Physical model

The flow of a dilute suspension of bubbles in a compressible liquid is modeled using
 ensemble phase averaging³⁵. This model is able to reproduce the correct bubbly-mixture
 sound speeds, nonlinear bubble dynamics, and their coupling to the suspending liquid^{1,2}.
 The mixture-averaged equations of motion are written in quasi-conservative form⁴:

$$\frac{\partial \mathbf{q}}{\partial t} + \nabla \cdot \mathbf{F} = \mathbf{0} \quad (2)$$

where $\mathbf{q} = \{\rho, \rho\mathbf{u}, E\}$ are the conservative variables and $\mathbf{F} = \{\rho\mathbf{u}, \rho\mathbf{u}\mathbf{u} + p\mathbf{I}, (E + p)\mathbf{u}\}$ are
 the fluxes. Here, ρ , \mathbf{u} , p , and E are the mixture density, velocity vector, pressure, and total

energy, respectively. The mixture pressure is

$$p = (1 - \alpha)p_l + \alpha \left(\frac{\overline{\mathbf{R}^3 \mathbf{p}_{bw}}}{\overline{\mathbf{R}^3}} - \rho \frac{\overline{\mathbf{R}^3 \dot{\mathbf{R}}^2}}{\overline{\mathbf{R}^3}} \right), \quad (3)$$

for which \mathbf{R} , $\dot{\mathbf{R}}$, and \mathbf{p}_{bw} are the radius, radial velocity, and wall pressure of the bubbles, respectively. These quantities are vectors that depend upon the equilibrium bubble sizes \mathbf{R}_o as $\mathbf{R}(\mathbf{R}_o) = \{R_1, R_2, \dots, R_{N_b}\}$, where $N_b = 31$ is the number of bins that describes the assumed log-normal distribution function of relative scale parameter σ^2 . Overbars $\bar{\cdot}$ denote the usual moments with respect to this distribution. Note that cases considered here are monodisperse unless stated otherwise, for which the bubble dynamic variables are scalars instead.

The liquid pressure p_l follows from the stiffened-gas equation of state as parameterized by the specific heat ratio γ_l and stiffness Π_∞^{24} . The void fraction is transported as

$$\frac{\partial \alpha}{\partial t} + \mathbf{u} \cdot \nabla \alpha = 3\alpha \frac{\overline{\mathbf{R}^2 \dot{\mathbf{R}}}}{\overline{\mathbf{R}^3}}, \quad (4)$$

where the right-hand-side represents the change of averaged bubble volume. The void fraction is transported as

The associated bubble dynamics are evaluated as

$$\frac{\partial n\phi}{\partial t} + \nabla \cdot (n\phi \mathbf{u}) = n\dot{\phi}, \quad (5)$$

where $\phi \equiv \{\mathbf{R}, \dot{\mathbf{R}}, \mathbf{p}_b, \mathbf{m}_v\}$ are the bubble dynamic variables, as will be described next, and n is the bubble number density per unit volume

$$n = \frac{3}{4\pi} \frac{\alpha}{\overline{\mathbf{R}^3}}. \quad (6)$$

- ¹⁴⁴ The bubbles are assumed to be spherical, ideal, and spatially uniform gaseous regions².
- ¹⁴⁵ Their dynamics are driven by pressure fluctuations of the surrounding liquid and their radial
- ¹⁴⁶ velocities and accelerations are computed via the Keller–Miksis equation¹⁶

$$R\ddot{R} \left(1 - \frac{\dot{R}}{c}\right) + \frac{3}{2}\dot{R}^2 \left(1 - \frac{\dot{R}}{3c}\right) = \frac{p_{bw} - p_\infty}{\rho} \left(1 + \frac{\dot{R}}{c}\right) + \frac{R\dot{p}_{bw}}{\rho c}, \quad (7)$$

where c is the sound speed, p_∞ is the bubble forcing pressure, and

$$p_{bw} = p_b - \frac{4\mu\dot{R}}{R} - \frac{2\sigma}{R} \quad (8)$$

- ¹⁴⁷ is the bubble wall pressure. The internal bubble pressure p_B and the mass of the bubble con-
- ¹⁴⁸ tents m_v follow from a reduced model that can represent heat and mass transfer²⁸. In whole,
- ¹⁴⁹ this single-bubble model includes thermal effects, viscous and acoustic ~~damping~~attenuation,
- ¹⁵⁰ and phase change.

¹⁵¹ C. Numerical methods

- ¹⁵² The model problem of figure 2 is spatially discretized via a rectilinear and uniformly
- ¹⁵³ spaced grid with $N = 3 \times 10^3$ grid points in each coordinate direction \hat{x} and \hat{y} , and thus
- ¹⁵⁴ $\Delta_x = \Delta_y = L/N$ are the mesh spacings. Non-reflective boundary conditions are used
- ¹⁵⁵ to minimize finite- L effects, though the principal results were found to be insensitive to
- ¹⁵⁶ doubling L and N . The numerical scheme used has been described in detail before⁵ and is
- ¹⁵⁷ integrated into the ~~MFC~~multi-component flow code (MFC), an open-source solver³. Thus,
- ¹⁵⁸ it is only briefly discussed here. The fluxes of (2) are split spatially and integrated within
- ¹⁵⁹ cell-centered finite volumes. The primitive variables are reconstructed at the finite-volume-

¹⁶⁰ cell faces via a 5th-order WENO-weighted essentially non-oscillatory (WENO) scheme⁵ and
¹⁶¹ the HLLC Harten, Lax, and van Leer contact (HLLC) approximate Riemann solver is used
¹⁶² to compute the fluxes³¹. The time derivative is computed using the 3rd-order TVD-total
¹⁶³ variation diminishing (TVD) Runge–Kutta algorithm¹² and the step size follows from the
¹⁶⁴ usual CFL-Courant-Friedrichs-Lowy (CFL) criterion, which is fixed at 0.1 based upon the
¹⁶⁵ speed of sound of water.

¹⁶⁶ **III. RESULTS**

¹⁶⁷ **A. Observation of wave guidance in an annular bubble net**

¹⁶⁸ The possibility of a acoustic waveguiding behavior in the model bubble net is considered
¹⁶⁹ first. Such wave guidance would entail a bending of incoming acoustic waves into the bubbly
¹⁷⁰ region from the exterior due to the change of sound speed, and subsequent reflection of the
¹⁷¹ waves back into this region when they reach the net inner wall¹⁸. For this, the configuration
¹⁷² of figure 2 (a), which represents a directional humpback whale vocalization grazing a bubble
¹⁷³ net, is simulated and then further parameter variations are discussed.

¹⁷⁴ Figure 3 shows the time evolution of a directional acoustic wave of grazing a bubble net
¹⁷⁵ for varying vocalization frequencies. For the lowest frequency considered $f = 1$ kHz, wave
¹⁷⁶ guidance is observed until $t = 8.1\delta/c_l$. This includes at least two reflections from the bubble
¹⁷⁷ net region that are clearly visible. However, this behavior is nominally steady state and
¹⁷⁸ no further guidance is observed. For $f = 2$ kHz the vocalization refracts towards the net
¹⁷⁹ center at $t = 2.7\delta/c_l$, though by $t = 5.4\delta/c_l$ no further wave guidance is observed. For

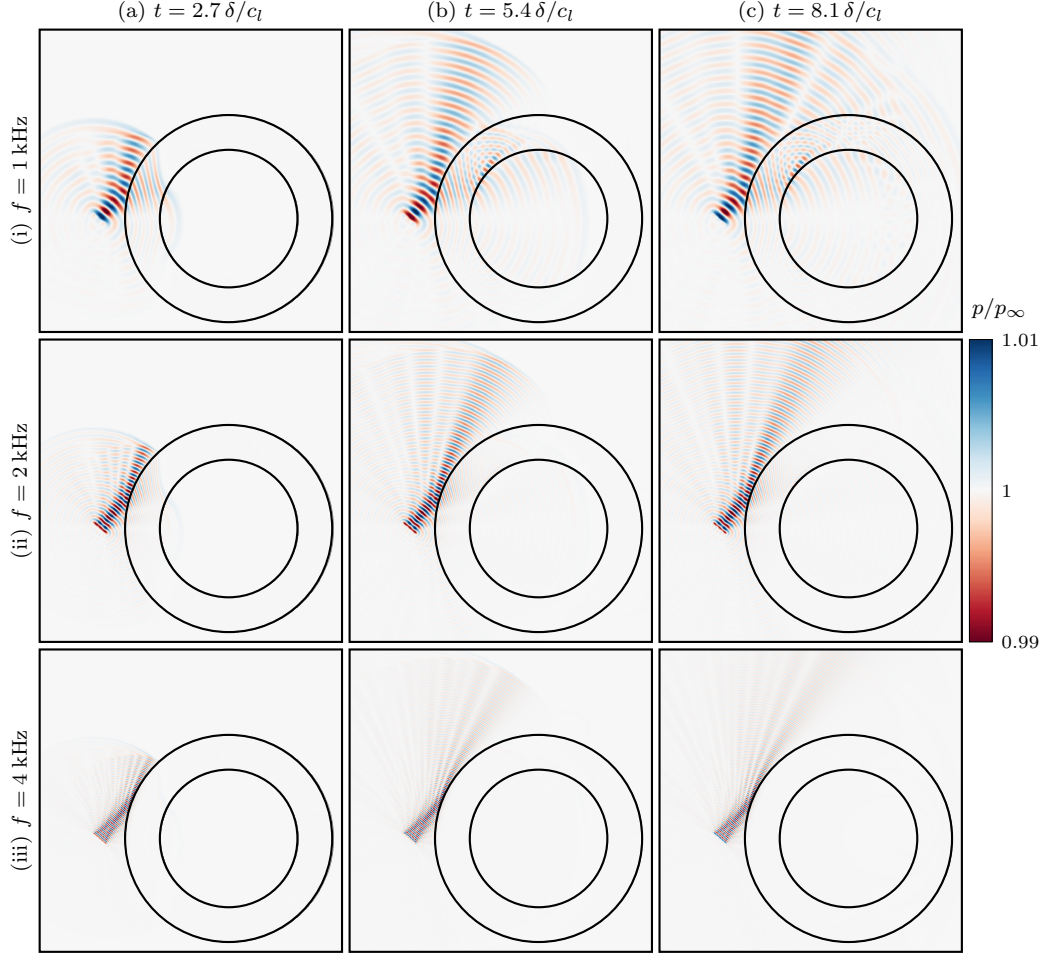


FIG. 3. Pressure p for bubble-net void fraction $\alpha_o = 10^{-4}$, (i)–(iii) varying monochromatic

acoustic source frequency f and of peak sound pressure level A at times (a)–(c) times. The

~~pressure scale corresponds to the maximum deviations from ambient pressure p_∞ due to a 180 dB pulse.~~ Times are non-dimensionalized by the net thickness δ and liquid sound speed c_l .

the highest frequency $f = 4$ kHz the effective impedance of the bubble wall is large and no

waves are observed in the bubbly region, though it was confirmed that decreasing α_o until

this impedance is small results in less wave-guidance than that observed for $f = 1$ kHz. The

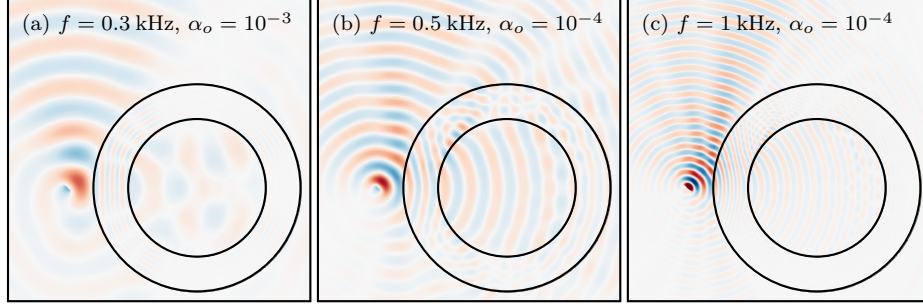


FIG. 4. Example $\sigma = 0.7$ polydisperse cases ~~with larger~~ ~~of varying~~ α_o and ~~smaller~~ f ~~as labeled~~.

Normalized pressure contours are shown.

¹⁸³ lack of continual wave-guidance, as was most pronounced in the $f = 1$ kHz case, appears to
¹⁸⁴ be due to the dispersion of the waves as they reflect in the non-uniform bubbly region.

¹⁸⁵ Considering monodisperse bubble populations means that, in order to optimally promote
¹⁸⁶ wave guidance, the resulting acoustic wave frequency must overlap with the single resonance
¹⁸⁷ frequency of the bubble population. This challenge can be partially alleviated by considering
¹⁸⁸ polydisperse bubble populations with a large span of such resonant frequencies. This is
¹⁸⁹ considered in figure 4, which uses a $\sigma = 0.7$ log-normally distribution of bubble sizes, as
¹⁹⁰ is considered typical for samples of sea water²⁷. Further, lower frequencies and larger void
¹⁹¹ fractions are also considered as a demonstration of waveguide potential Figure 4 (a) show
¹⁹² a $f = 0.3$ kHz case with larger $\alpha_o = 10^{-3}$ void fraction. For this case the wavelength
¹⁹³ of the exciting frequency exceeds δ , thus prohibiting wave-guidance. The $f = 0.5$ kHz,
¹⁹⁴ $\alpha_o = 10^{-4}$ case of figure 4 (b) shows that further decreasing f from the previous cases
¹⁹⁵ considered results in ~~a significant pollution~~ ~~significant acoustic excitation~~ of the bubble-net
¹⁹⁶ center. This, combined with the lack of additional waveguiding observed, suggests that such
¹⁹⁷ a configuration is less effective for this feeding strategy. Finally, in figure 4 (c) an otherwise

198 previously considered case is shown, with the exception of the polydispersity and smaller
199 acoustic source width of $L_a = 0.2r_o$ (representing the possibility of a parametric sonar-like
200 effect²²). Again, modifying these parameters does not promote waveguiding, seemingly due
201 to the significant dispersion observed in the bubbly region. Further, varying the bubble-net
202 thickness (δ), grazing angle (θ), location, and amplitude (A) of the incoming vocalizations
203 did not observe wave-guidance beyond about two reflections from the bubble-net wall.

204 Thus, these results support prior claims that in practice the annular bubble net likely does
205 not reliably act as a waveguide¹⁷. Of course, additional whales carefully organized around
206 the net and vocalizing in a similar fashion could promote excitation of the bubbly region.
207 However, if several whales are present and cooperating, it might be more likely that they
208 are exploiting a more simple mechanism: they are utilizing the bubble net as an acoustic
209 shield. This possibility is investigated next.

210 **B. Acoustic shielding of annular bubble nets**

211 Multiple whales vocalizing towards a bubble net are modeled via the configuration of
212 figure 2 (b). The flow is simulated until a steady state is reached and the resulting acoustic
213 waves are visualized and analyzed.

214 The pressure p is A stationary standing wave pattern is formed at long times. Examples
215 of such wave patterns are shown in figure 5 for varying configurations. At long times a
216 spatial pattern in p emerges, which This pattern changes qualitatively as the waves enter
217 the annular region and the net interior. The azimuthal periodicity of these patterns results
218 from the in-phase acoustic excitation of the line sources. Out-of-phase acoustic excitation

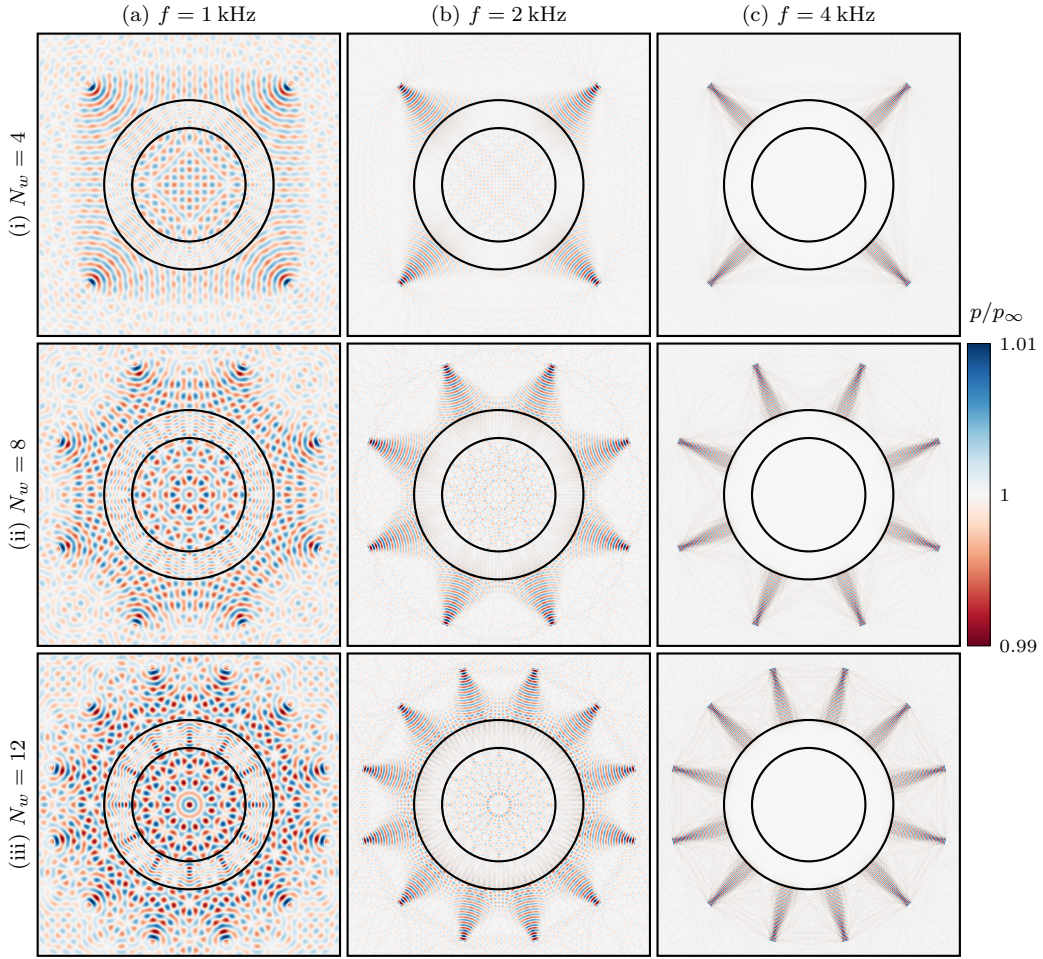


FIG. 5. Long-time ($t = 50\delta/c_1$) pressure p for $\alpha_o = 10^{-4}$ and (a)–(c) varying acoustic source frequency f and (i)–(iii) their number N_w as labeled.

²¹⁹ is not considered here, since the in-phase case results in maximum constructive interference
²²⁰ between the line sources. For $N_w = 8$ and 12, the pressure contours are circular at the
²²¹ bubble-net center, though for $N_w = 4$ no such pattern feature is seen. Further, as f increases,
²²² the bubble net increasingly shields the interior from the acoustic sources and the interior
²²³ acoustic waves diminish in magnitude; for $f = 4 \text{ kHz}$ a pattern cannot be discerned. For
²²⁴ increasing N_w the amplitude of p generally increases, though the penetration of the waves

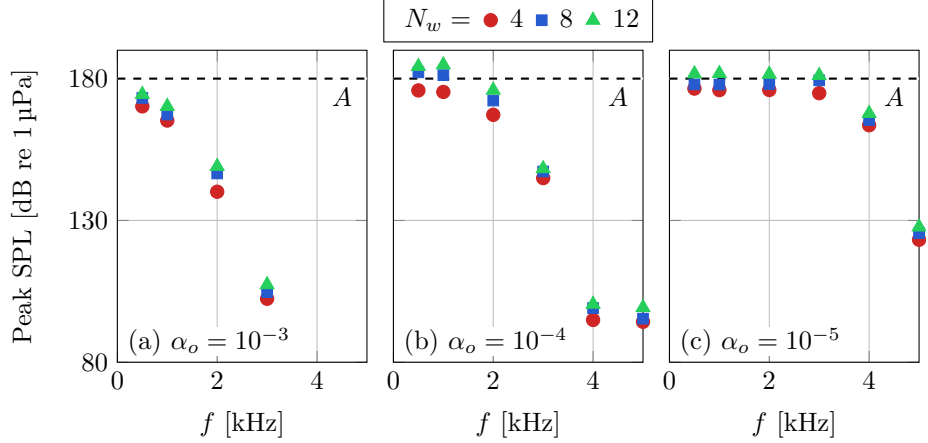


FIG. 6. Maximum Peak sound pressure level (SPL_{\max}) within the bubble-net interior for varying f and N_w , and net void fractions (a)–(c) α_o as labeled.

are most closely coupled to their frequency as the $N_w = 12$ and $f = 4$ kHz case still does not noticeably penetrate the bubble net.

Figure 6 shows the loudness of the bubble net interior for varying vocalization frequencies, number of sources, and net void fractions. Here, SPL_{\max} is computed as the usual maximum peak sound pressure level (SPL) within the bubble net interior after $t = 50\delta/c_l$ (after which they vary $< 1\%$) for several example cases. Consistent with the visualizations of figure 5, the interior loudness peak SPL generally decreases with increasing f and decreasing N_w . For $\alpha_o = 10^{-4}$, the peak SPL decreases with increasing f until $f = 4$ kHz, after which it is nearly constant. For the more dilute $\alpha_o = 10^{-5}$ cases, the peak SPL is nearly constant with increasing f until $f = 4$ kHz, at which point it decreases significantly. For the less dilute $\alpha_o = 10^{-3}$, the loudness peak SPL decreases a similar degree to the $\alpha_o = 10^{-4}$ cases, though for a lower $f = 3$ kHz.

237 If whales are to leverage these nets to shield and corral prey, then a ~~small SPL_{max}/A is~~
238 ~~likely required to keep significant reduction in the peak SPL observed within the net from~~
239 ~~that of the incoming acoustic waves is required to maintain~~ the bubble net interior as an
240 attractive location. ~~If $SPL_{max} = 0.5A$~~ For example, if a net interior peak SPL of 90 dB re
241 ~~1 μPa~~ is used as a ~~nominal~~ threshold for this, then the whales must generate nets with
242 $\alpha_o \gtrsim 10^{-4}$ to sufficiently ~~damp attenuate~~ their $A = 180$ dB re ~~1 μPa~~ vocalizations. Nets
243 with a void fraction this high have the additional advantage that they serve to physically
244 trap small fish, as previously documented for bubble curtains¹⁰. However, this configuration
245 only makes sense when multiple whales are present, since multiple sources are required to
246 surround the next with sound. A seemingly more robust spiral-net configuration that is
247 amenable to single-whale hunting is investigated next.

248 C. Spiral-shaped bubble nets

249 As discussed in section I, spiral-shaped bubble nets have been proposed as a possible
250 configuration for trapping prey²⁰. Such spiral nets are considered next, including variation
251 of net void fractions and exciting acoustic frequencies. This serves to clarify the possible
252 acoustic mechanisms that could be present in this flow configuration. Further, it works to
253 resolve the parameterizations that promote robust feeding strategies. —

254 Figure 7 shows example acoustic-spiral-bubble-net interactions for a range of vocaliza-
255 tion frequencies and times. For frequencies that correspond to wavelengths larger than the
256 bubble-free-arm spacing, e.g. the $f = 0.1$ kHz case shown here, the waves propagate around
257 the spiral as if in a duct, with only minor attenuation due to interactions with the bubble-net

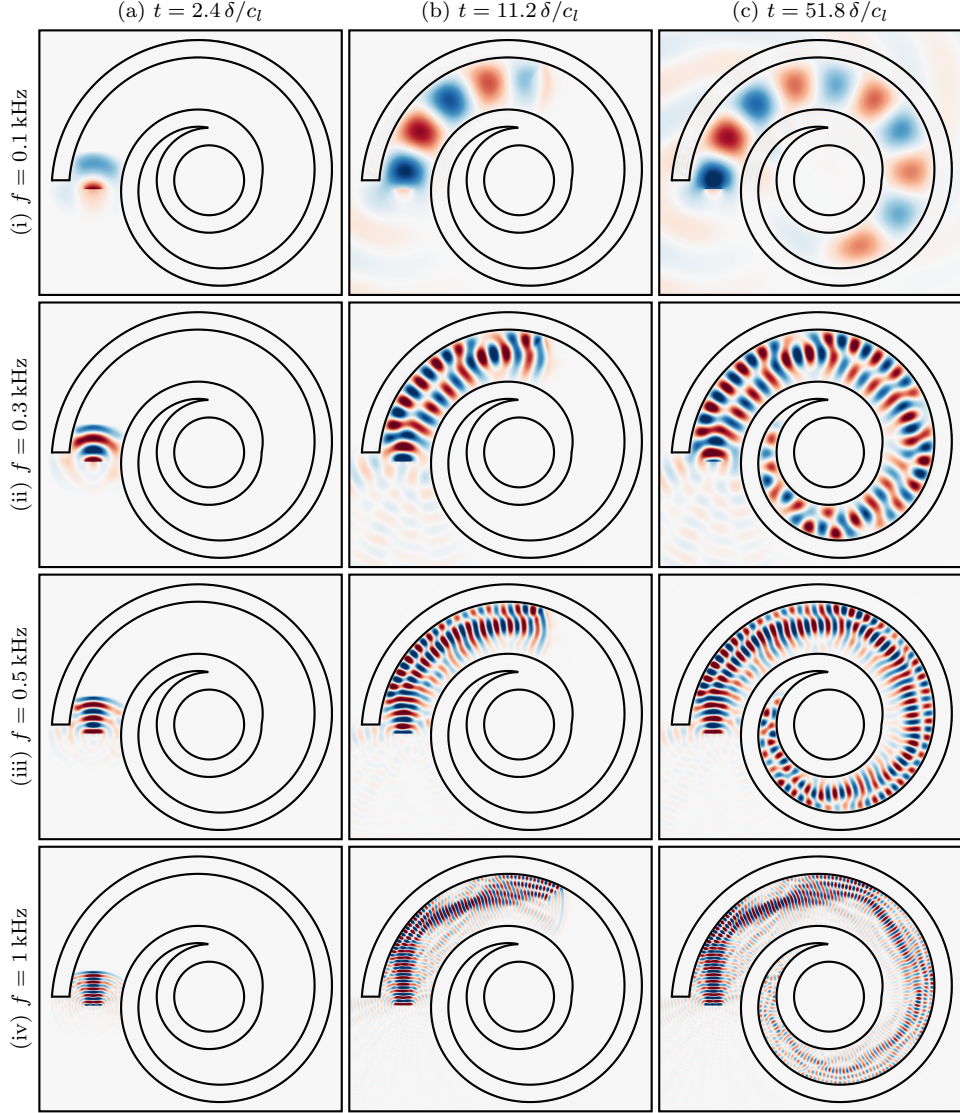


FIG. 7. Acoustics in a $\alpha_o = 10^{-2}$ spiral bubble net for (i)–(iv) vocalization frequency f at (a)–(c)

times t . The normalized sound pressure level p/p_∞ is shown using the same scale as figures 3 and 5.

258 wall. For the $f = 0.3$ kHz case of figure 7 (ii) a different behavior is observed. The vocaliza-
 259 tion reflects at the bubble-wall, introducing two coherent wave patterns of similar amplitude
 260 in the constant-width portion of the bubble-free region. This interference pattern changes
 261 in the narrowing-portion of the arm, though the wave amplitudes remain similar. Thus, the

262 entire bubble-free region is excited at a nearly constant amplitude. For the $f = 0.5$ kHz
263 case a similar interference pattern is observed in the constant-width portion of the spiral,
264 though the ever decreasing grazing angle of the reflected waves results in a quieter layer
265 near the spiral center, consistent with the ray-tracing results of Leighton *et al.*²¹. For the
266 $f = 1$ kHz case the directionality of the acoustic waves are apparent from the first time
267 shown, figure 7 (a,iv). In this case the amplitude of the waves attenuates more rapidly due
268 to reflection and transmission at the bubble-net wall. Further, an effectively quiet route of
269 escape from the net center exists due to the directionality of the acoustic reflections. Of
270 course, variations in source directions and locations could at least partially collapse this re-
271 gion. However, this remains a disadvantage of the high- f cases when compared to the lower
272 f cases that fully surround the center in loud vocalizations. For these reasons, higher f are
273 not considered for this configuration. Note that only monodisperse cases were considered for
274 these cases. This is because the high impedance mismatch at the bubble-net wall results in
275 relatively little wave transmission. Further, polydispersity only introduced a modest effect
276 on the refraction-dominated waveguiding observed in figure 4.

277 From the visualizations it is anticipated that α_o and f have competing effects on the
278 ability of the bubble net to both guide and protect the central bubble-free region from vo-
279 calizations. These effects are first quantified in figure 8 by measuring as the averaged sound
280 pressure SPL_{avg} level in four $0.2r_o$ -thick patches located along the bubble-free spiral por-
281 tion of the net. Patches 1–4 are centered at $(-3r_o, 0)$, $(0, 2.5r_o)$, $(2r_o, 0)$, and $(0, -1.75r_o)$,
282 respectively, and the averaged SPL is computed as the spatially-averaged maximum sound
283 pressure at some time t , from which the averaged SPL is computed. This spatially-averaged

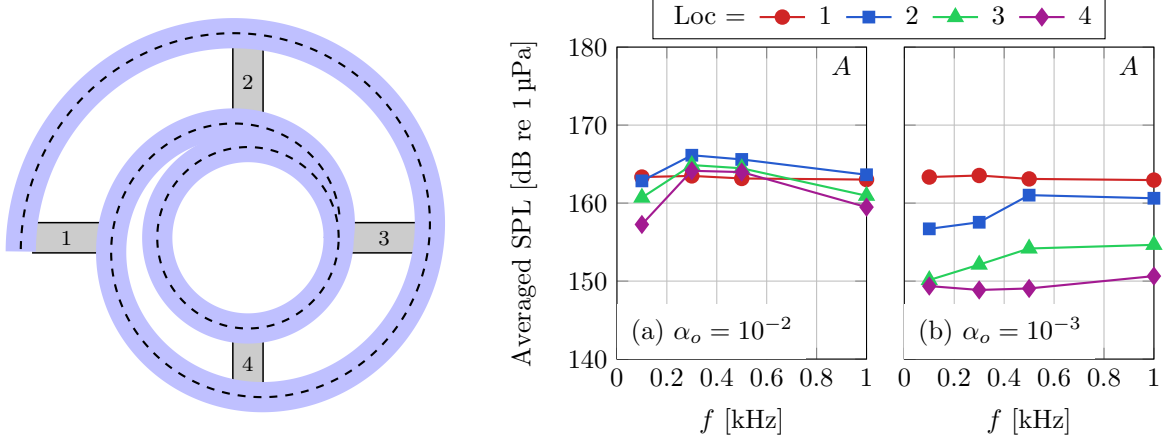


FIG. 8. ~~Spatially averaged long-time~~ ~~Spatially- and temporally-averaged~~ sound pressure level

SPL_{avg} in the labeled regions 1–4 for (a) $\alpha_o = 10^{-2}$ and (b) $\alpha_o = 10^{-3}$.

284 ~~SPL is time-averaged over $t \in (15, 25)r_o/c_l$.~~ As expected, ~~SPL~~_{avg} ~~the averaged sound pressure~~
 285 ~~level~~ at location 1, prior to significant interaction with the bubble wall, is effectively inde-
 286 pendent of f for both α_o .

287 For the higher void-fraction case ($\alpha_o = 10^{-2}$), ~~SPL~~_{avg} ~~the averaged SPL~~ is similar for all
 288 4 locations along the spiral, as there is greater internal reflection and smaller transmission
 289 due to the high impedance mismatch. For the lower volume fraction case ($\alpha_o = 10^{-3}$), where
 290 the impedance mismatch is smaller, there is greater transmission of waves and consequently
 291 a significant reduction in ~~SPL~~_{avg} ~~the averaged SPL~~ along the spiral. These results are
 292 independent of f , with only minor variations due to differing spatial wave patterns within
 293 the spiral over the range of frequencies considered.

294 The $\alpha_o = 10^{-3}$ cases were shown to allow a portion of the vocalizations to escape the
 295 bubble net entirely, which decreased their measured amplitude as they propagate around
 296 the spiral. However, this lower α_o also means that the remaining waves can more easily

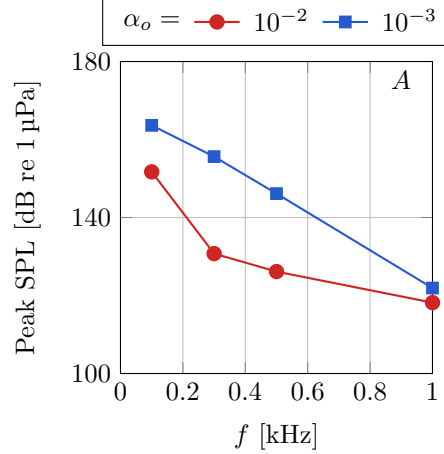


FIG. 9. Maximum sound pressure level SPL_{\max} in the bubble-net center for varying monochromatic excitation of frequency f and void fractions (a) $\alpha_o = 10^{-2}$ and (b) $\alpha_o = 10^{-3}$.

penetrate the central bubble net region, where the prey are corralled. Figure 9 illustrates this trade-off via the maximum sound pressure level in the bubble-net center for varying α_o and f . For $f < 1 \text{ kHz}$, the peak SPL is significantly smaller for the $\alpha_o = 10^{-2}$ than 10^{-3} cases. Thus, even though a portion of the wave can escape the spiral net for the $\alpha_o = 10^{-3}$ cases, it still remains louder in the central bubbly-free region. As a result, the $\alpha_o = 10^{-2}$ configurations are preferable for these f in terms of both surrounding the entire net with loud vocalizations and keeping the interior quiet. For $f = 1 \text{ kHz}$ similar SPL_{\max} peak SPL are observed for both α_o . This is due to the trade-off between increased refraction in the bubbly arm of the spiral and the inability of these higher frequencies to penetrate the central net annulus. This behavior is expected for still higher f due to the directionality of the waves in this regime.

Thus, for low-frequency $f \lesssim 1 \text{ kHz}$ vocalizations, a higher $\alpha_o \gtrsim 10^{-2}$ void fraction is preferable in order to keep the waves in the bubble-net spiral. For higher frequencies $f \gtrsim$

310 1 kHz, SPL_{\max} the peak SPL observed is relatively insensitive to α_o and thus this parameter is
311 less important. However, as was shown in figure 7, the directionality of these high frequency
312 vocalizations means that a quiet region can form at the interior layer of the spiral, leaving
313 the prey a possible escape route.

314 IV. DISCUSSION AND CONCLUSIONS

315 As a step towards fully understanding the complex humpback whale bubble-net feeding
316 process three possible acoustic mechanisms were assessed: wave-guidance and bubble-wall
317 shielding for annular nets and vocalization guiding for spiral configurations. For this, a fully-
318 coupled compressible bubbly flow model capable of representing the modified mixture speed
319 of sound, geometric effects of the curved bubble wall, and nonlinear and collective bubble
320 dynamics was used. This model was solved using a high-order interface capturing scheme
321 that minimized spurious oscillations near material interfaces. A configuration of acoustic-
322 generating sources and bubbly regions was used as a model of actual vocalizing humpback
323 whales and the bubble nets they generate. Simulations of this system were analyzed and
324 connected to observed whale feeding phenomena.

325 A wave-grazing flow configuration was considered to determine if waveguiding in the
326 bubbly region could efficiently keep the bubbly region loud. Analysis showed that for the
327 parameterizations considered only modest waveguiding could be observed. This was most
328 prominent for relatively low frequencies ($f = 1 \text{ kHz}$), but still only encompassed less than
329 half of the bubble net. To ensure that this was not due to the model parameterization, this
330 conclusion was shown to be unchanged when considering bubble population polydispersity,

³³¹ varying bubble-net thickness, acoustic frequencies, and their directionality, breadth, and
³³² amplitude.

³³³ A configuration representing multiple vocalizing whales was used to quantify the attenua-
³³⁴ tion and acoustics of an annular bubble-net and the region that surrounded it. Qualitatively
³³⁵ different acoustic patterns were observed, depending upon the number of whales present.
³³⁶ The degree of attenuation was most strongly dependent on the frequency of the vocaliza-
³³⁷ tions, with significant attenuation of the 180 dB waves down to about 90 dB for a range of
³³⁸ cases that overlapped with possible whale vocalization frequencies and net void fractions.
³³⁹ This suggests that it is possible humpback whales utilize these bubbly regions as a shield,
³⁴⁰ but only if multiple whales are cooperating.

³⁴¹ The weakness of the acoustic shielding hypothesis is associated with the required number
³⁴² of cooperating whales to utilize it. A previously proposed spiral bubble net configuration
³⁴³ that could be utilized by a single whale was also considered²⁰. Indeed, observations suggest
³⁴⁴ that the shape might be closer to spiral than annular. With a single model whale vocalizing
³⁴⁵ into the bubble-free end of the spiral net, the guidance of the acoustic waves through the
³⁴⁶ spiral was observed. However, their behavior depended upon the vocalization frequency and
³⁴⁷ net void fraction. For example, vocalizations of wavelengths near the width of the bubble-
³⁴⁸ free arm were simply guided through this region, without noticeable reflection at the bubble
³⁴⁹ walls, whereas higher frequency cases displayed varying degrees of reflections and, thus,
³⁵⁰ **loudness** sound pressure level as they propagated through the spiral. Importantly, for nets
³⁵¹ with smaller void fractions, low frequency vocalizations were able to penetrate the bubble
³⁵² arm, reducing their magnitude when they reach the central bubble net region. For higher

353 frequencies, both reflection and refraction and the bubble-net walls resulted in a directional
354 acoustic behavior at ever decreasing grazing angles. These cases kept the most of the bubble-
355 free region loud, though for sufficiently high frequencies a quiet region for the model prey to
356 escape exist. This set of competing effects was, in part, quantified by the maximum sound
357 pressure level observed in the bubble-net center. This metric suggested that the higher
358 void-fraction $\alpha_o = 10^{-2}$ nets considered were superior to the $\alpha_o = 10^{-3}$ cases, even though
359 they guided the entirety of the whale vocalizations towards the bubble-net center.

360 Additional field observations are required to further clarify the space of possible con-
361 figurations. For example, the exact spatial locations and directions of the whales during
362 feeding would better illuminate their behaviors. A better estimation of the expected bubble
363 void fractions in the nets could also possibly rule out acoustic mechanisms or vocalization
364 frequencies, since this parameter was intimately related to the viability of the configurations
365 considered.

366 ACKNOWLEDGMENTS

367 We thank Dr. Kevin Schmidmayer for numerous fruitful discussions. This work was
368 supported by the Office of Naval Research under grant number N0014-17-1-2676. Associated
369 computations utilized the Extreme Science and Engineering Discovery Environment, which
370 were supported by the US National Science Foundation under grant number TG-CTS120005.

³⁷¹ REFERENCES

- ³⁷² ¹Ando, K. (2010). “Effects of polydispersity in bubbly flows,” Ph.D. thesis, California
³⁷³ Institute of Technology.
- ³⁷⁴ ²Bryngelson, S. H., Schmidmayer, K., and Colonius, T. (2019). “A quantitative comparison
³⁷⁵ of phase-averaged models for bubbly, cavitating flows,” Int. J. Mult. Flow **115**, 137–143.
- ³⁷⁶ ³Bryngelson, S. H., Schmidmayer, K., Coralic, V., Meng, J. C., Maeda, K., and Colonius, T.
³⁷⁷ (2019). “MFC, an open-source high-order multi-component, multi-phase, and multi-scale
³⁷⁸ compressible flow solver,” arXiv **1907.10512**.
- ³⁷⁹ ⁴Commander, K. W., and Prosperetti, A. (1989). “Linear pressure waves in bubbly liquids:
³⁸⁰ Comparison between theory and experiments,” J. Acoust. Soc. Am. **85**(732).
- ³⁸¹ ⁵Coralic, V., and Colonius, T. (2006). “Finite-volume WENO scheme for viscous compress-
³⁸² ible multicomponent flow problems,” J. Comp. Phys. **219**(2), 715–732.
- ³⁸³ ⁶Domenico, S. N. (1982). “Acoustic wave propagation in air-bubble curtains in water–Part
³⁸⁴ I: History and theory,” Geophysics **47**, 345–353.
- ³⁸⁵ ⁷Duke Marine Lab (2018). “Highlights from Antarctica research” File: “<https://sites.nicholas.duke.edu/uas/highlights-from-antarctica-research>”.
- ³⁸⁷ ⁸D’Vincent, C. G., Nilson, R. M., and Hanna, R. E. (1985). “Vocalization and coordinated
³⁸⁸ feeding behavior of the humpback whale in southeastern Alaska,” Sci. Rep. Whales Res.
³⁸⁹ Inst. **36**, 41–47.
- ³⁹⁰ ⁹Evadb (2007). “Whales bubble net feeding” Public domain, File: “https://commons.wikimedia.org/wiki/File:Whales_Bubble_Net_Feeding.jpg”.

- ³⁹² ¹⁰Finley, L. A., Nicol, S., and MacMillan, D. L. (2003). “The effectiveness of a bubble curtain
³⁹³ for preventing physical damage to antarctic krill in captivity,” Mar. Freshw. Behav. Phy.
³⁹⁴ **36**(4), 285–293.
- ³⁹⁵ ¹¹Fish, F. E., and Battle, J. M. (1995). “Hydrodynamic design of the humpback whale
³⁹⁶ flipper,” J. Morphol. **225**, 51–60.
- ³⁹⁷ ¹²Gottlieb, S., and Shu, C.-W. (1998). “Total variation diminishing Runge–Kutta schemes,”
³⁹⁸ Math. Comput. **67**(221), 73–85.
- ³⁹⁹ ¹³Hain, J. H. W., Carter, G. R., Kraus, S. D., Mayo, C. A., and Winn, H. E. (1982).
⁴⁰⁰ “Feeding behavior of the humpback whale, *Megaptera novaeangliae*, in the western North
⁴⁰¹ Atlantic,” Fishery Bull. **8**(2), 259–268.
- ⁴⁰² ¹⁴Ingebrightsen, A. (1929). “Whales caught in the North Atlantic and other seas,” Int. Counc.
⁴⁰³ Explor. Sea, Rapp. P.-V. Réun (56), 1–26.
- ⁴⁰⁴ ¹⁵Jurasz, C., and Jurasz, V. (1979). “Feeding modes of the hupmback whale, *Megaptera*
⁴⁰⁵ *novaeeangliae*, in southeastern Alaska,” Sci. Rep. Whales Res. Inst. **31**, 69–83.
- ⁴⁰⁶ ¹⁶Keller, J. B., and Miksis, M. (1980). “Bubble oscillations of large amplitude,” J. Acoust.
⁴⁰⁷ Soc. Am. **68**(628).
- ⁴⁰⁸ ¹⁷Leighton, T. G. (2004). “From seas to surgeries, from babbling brooks to baby scans: The
⁴⁰⁹ acoustics of gas bubbles in liquids,” Int. J. Mod. Phys. B **18**(25), 3267–3314.
- ⁴¹⁰ ¹⁸Leighton, T. G. (2004). “Nonlinear bubble dynamics and the effects on propagation
⁴¹¹ through near-surface bubble layers,” in *AIP Conf. Proc.*, edited by W. K. M. B. Porter,
⁴¹² M. Siderius, High-Frequency Ocean Acoustics (American Institute of Physics Melville,

- 413 New York), Vol. 728, p. 180.
- 414 ¹⁹Leighton, T. G., Finfer, D., Grover, E., and White, P. R. (2007). “An acoustical hypothesis
415 for the spiral bubble nets of humpback whales and the implications for whale feeding,” in
416 *Acoustics Bulletin*, Vol. 22, pp. 17–21.
- 417 ²⁰Leighton, T. G., Finfer, D. C., Grover, E. J., and White, P. R. (2007). “Spiral bubble
418 nets of humpback whales: An acoustic mechanism,” in *2nd Int. Conf. & Exhibition on*
419 *“Underwater Acoustic Measurements: Technologies & Results”*, pp. 583–588.
- 420 ²¹Leighton, T. G., Finfer, D. C., and White, P. R. (2007). “Cavitation and cetacean,”
421 Revista de Acustica **38**(3/4), 37–81.
- 422 ²²Leighton, T. G., Richards, S. D., and White, P. R. (2004). “Trapped within a “wall of
423 sound”,” in *Acoustics Bulletin*, Vol. 29, pp. 24–29.
- 424 ²³Leighton, T. G., and White, P. R. (2014). “Dolphin-inspired target detection for sonar
425 and radar,” Arc. Acoust. **38**(3), 319–332.
- 426 ²⁴Menikoff, R., and Plohr, B. J. (1989). “The Riemann problem for fluid-flow of real mate-
427 rials,” Rev. Mod. Phys. **61**(1), 75–130.
- 428 ²⁵Mercado, E., and Frazer, L. N. (1999). “Environmental constrains on sound transmission
429 by humpback whales,” J. Acoust. Soc. Am. **106**(5), 3004–3016.
- 430 ²⁶Mercado, E., and Frazer, L. N. (2001). “Humpback whale song or humpback whale sonar?
431 A reply to Au et al.,” IEEE J. Ocean. Eng. **26**(3), 406–415.
- 432 ²⁷O’Hern, T. J., d’Agostino, L., and Acosta, A. J. (1988). “Comparison of holographic and
433 coulter counter measurements of cavitation nuclei in the ocean,” J. Fluids Eng. **110**(200–

- 434 207).
- 435 ²⁸Preston, A., Colonius, T., and Brennen, C. E. (2007). “A reduced-order model of diffusion
436 effects on the dynamics of bubbles,” Phys. Fluids **19**(123302).
- 437 ²⁹Sharpe, F. A., and Dill, L. M. (1997). “The behaviour of Pacific herring schools in response
438 to artificial humpback whale bubbles,” Can. J. Zool. **75**, 725–730.
- 439 ³⁰Thompson, P. O., Cummings, W. C., and Ha, S. J. (1986). “Sounds, source levels, and
440 associated behavior of humpback whales, Southeast Alaska,” J. Acoust. Soc. Am. **80**(3),
441 735–740.
- 442 ³¹Toro, E., Spruce, M., and Speares, W. (1994). “Restoration of the contact surface in the
443 HLL-Riemann solver,” Shock waves **4**(1), 25–34.
- 444 ³²Valsecchi, E., Corkeron, P., and Amos, W. (2002). “Social structure in migrating hump-
445 back whales (*Megaptera novaeangliae*),” Mol. Ecol. **11**(3), 507–513.
- 446 ³³Wiley, D., Ware, C., Bocconcini, A., Cholewiak, D., Friedlaender, A., Thompson, M., and
447 Weinrich, M. (2011). “Underwater components of humpback whale bubble-net feeding
448 behaviour,” Behaviour **148**(5–6), 575–602.
- 449 ³⁴Würsig, B., Greene Jr., C. R., and Jefferson, T. A. (2000). “Development of an air bubble
450 curtain to reduce underwater noise of percussive piling,” Mar. Environ. Res. **49**(1), 79–93.
- 451 ³⁵Zhang, D. Z., and Prosperetti, A. (1994). “Ensemble phase-averaged equations for bubbly
452 flows,” Phys. Fluids **6**(2956).